TOPICS IN ISOCAM SPECTROSCOPY CALIBRATION*

A. Biviano[1,2]

[1]ISO Science Operations Centre, Astrophysics Division, Space Science Department of ESA, Villafranca, P.O. Box 50727, 28080 Madrid, Spain

[2]Istituto Te.S.R.E., Area della Ricerca del CNR, via Gobetti 101, I-40129 Bologna, Italy

ABSTRACT

I present here the current status of calibration of the Circular Variable Filters (CVF) of the ISO-CAM instrument. Specifically, I address the topics of the Spectral Response Function (SRF hereafter), of spectral purity (i.e. the wavelength calibration), and of ghost images.

CVF photometry on a single star is shown to be repeatable at a level of ~ 2 % The rms uncertainty on the SRF, calibrated using several stars, is ~ 4 %.

There are two kinds of ghosts in the CVF images, one comoving with the source image, the other moving symmetrically with respect the array center. Preliminary estimates of the ghost photometry and spectra are given.

For what concerns the spectral purity, the measured spectral lines of several sources are shown to fall into the expected CVF step positions, when the image of the source is centered in the middle of the array. When the source image is at the edge of the array, there is a wavelength shift that depends on the wavelength itself, and may go up to 0.1 μm.

Key words: instrument calibration; macros; LaTeX.

1. INTRODUCTION

Spectroscopy with ISO-CAM means observing with the Circular Variable Filters (CVF hereafter). I refer to the "ISOCAM Observer's Manual" for a full description of the CVF.

The CVF covers the wavelength range from 2.273 μm to 17.34 μm with three segments, one in the SW channel of CAM and two in the LW channel, using 285 step positions.

The advantage of using the CVF is that it allows spectro-imagery with a high sensitivity. On the other hand, the resolution is limited to about $\lambda/\delta\lambda \simeq 40$.

*ISO is an ESA project with instruments funded by ESA Member States (especially the PI countries: France, Germany, the Netherlands and the United Kingdom) and with the participation of ISAS and NASA

In this paper, I resume the current status of the CVF calibration, as obtained "in-orbit" from dedicated calibration observations. In § 2. I describe the calibration of the Spectral Response Function (SRF hereafter); in § 3. I describe our current understanding of the properties of the ghost images that affect CVF observations; in § 4. I deal with the wavelength calibration of the CVF, the so-called "spectral purity".

2. THE SPECTRAL RESPONSE FUNCTION

The main calibration stars for the determination of the SRF of the SW and LW CVFs are HIC96441 and HIC94376 (δ Draconis), respectively. Other stars have been observed as well, however, to check that the derived SRF is independent on the received flux.

The repeatability of the CVF photometry *on the same star* is excellent, ± 3 % rms, whatever the pixel-field-of-view (PFOV hereafter) used. On the other hand, it is wiser to use more than one star for deriving the SRF, in order to check that the SRF is the same for different flux levels, and to minimize possible systematic errors in the models to which our observation are confronted. The rms is likely to be a little bit larger when more than a single star are considered (see below).

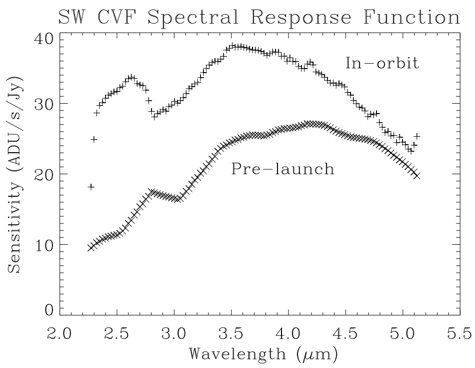

Figure 1. The pre-launch and in-orbit estimates of the SW CVF SRF (X's and crosses, respectively).

In Fig.1 and 2 I have plotted the SRFs of the SW and, respectively, the LW CVFs (note that the two segments of the LW CVF are plotted together). In these figures I show both the pre-launch estimates of the SRFs and

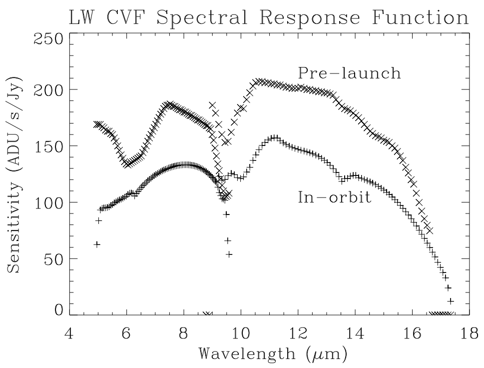

Figure 2. The pre-launch and in-orbit estimates of the LW CVF SRF (X's and crosses, respectively). Both segments of the LW CVF (CVF1 and CVF2) are shown.

the current estimates of the SRFs. It can be seen that the SW SRF has a higher sensitivity than expected from pre-launch measurements. It is 3 times more sensitive at short wavelengths and approximately as sensitive at long wavelengths. On the other hand, the LW CVF sensitivity is only 0.7 the pre-launch estimation, on average, although also in this case, it appears to be more similar to the pre-launch estimation at long wavelengths.

It must be pointed out that the CVF photometry has been applied with no correction for the Point-Spread-Function (PSF hereafter), because the PSFs for the CVF were not available at the time of the CVF data-reduction. Recently, PSFs at several CVF steps have been observed. Unfortunately, and as expected, they differ from the the theoretical PSF, because they include a ghost image from the star (see § 3.). It is therefore not yet possible to apply a PSF correction to the CVF photometry without properly accounting for the ghost images as well.

We can nevertheless use the theoretical PSF just to have a feeling of how the SRFs would be modified after a PSF correction. Generally, the correction will be larger at longer wavelengths, and will make the sensitivity higher, since part of the flux is outside the aperture we used for deriving CVF photometry. This correction brings the ratio between the pre-launch and in-orbit LW SRFs to 0.8, thus reducing the difference, but not completely, but does not help in reducing the difference between the pre-launch and in-orbit SW SRF. As we will see in § 3., the residual 20 % discrepancy between the pre-launch and in-orbit LW SRFs is probably due to the flux lost in the ghost image.

The error bars of the derived CVF SRFs are shown in Fig. 3 (SW CVF), Fig. 4 (LW CVF1) and Fig. 5 (LW CVF2), along with the SRFs themselves. These error bars represent the RMS among different measurements used for deriving the SRFs, and do not include any systematic errors, such as those coming from not applying the PSF correction (see above) or from the presence of ghosts (see § 3.). The average random error of the SW CVF SRF is $\sim$ 5 %, but in some SW CVF position the error is as large as 18 %, especially at large wavelengths, where the calibrating star flux is lower. The RMS of the LW CVF1 SRF is 4 %, on average, and always $<$ 20 %, except for the very last CVF step position at long wavelength, where the SRF is essentially undetermined, because the RMS is $\sim$ 100 % of the measured value. Fortunately, the same wavelength is also covered by the LW CVF2, with a much better accuracy. Overall, the RMS of the CVF2

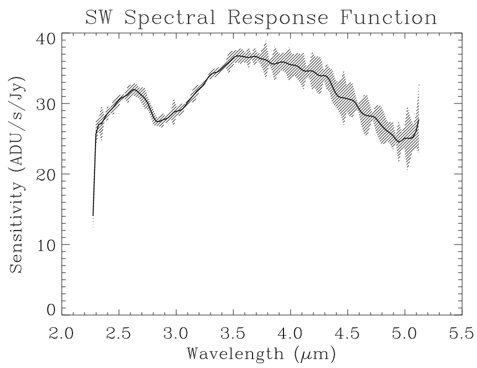

Figure 3. The SW CVF SRF within its $\pm 1\sigma$ confidence r (shaded region), where σ is the RMS obtained from the several measurements used to obtain the SRF.

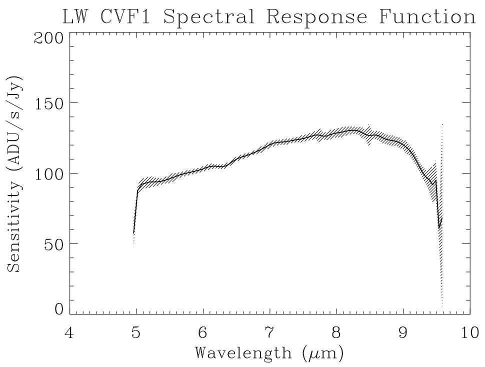

Figure 4. The LW CVF1 SRF within its $\pm 1\sigma$ confidence (shaded region), where σ is the RMS obtained from the several measurements used to obtain the SRF.

SRF is 4 %, on average, and $<$ 10 % at all CVF positions available to the observer, i.e. from 9.003 to 16.52 μm (see the "ISOCAM Observer's Manual"). The SRF at CVF positions outside the recommended range is affected by much larger errors (average of 22 % and up to 73 %). The SRF of these CVF positions has been calibrated for completeness.

2.1. Effects of stabilization

Part of the scatter in the CVF SRF probably comes from incomplete stabilization. The CVF scan observations are very time consuming so that it is impossible to spend more than $\sim$ 20 frames per position within the available calibration time (as an example, a full scan of the SW CVF at 2 sec integration time with 20 frames per position requires 1.3 hours).

In Fig. 6 we show the signal time histories of the brightest pixel of the HIC96441 star image, observed at the first SW CVF position at the beginning and at the end of a forth+back scan. Stabilizing trends can clearly be seen. When the star is observed the first time at the first CVF scan position, an upwards stabilizing behaviour can be seen, due to the fact that the pixel signal is stabilizing from a low to a high flux level. A hundred frames were spent on this first position, with the purpose of allowing a stabilized signal to be reached. However, all following CVF steps were done with only 20 frames, for

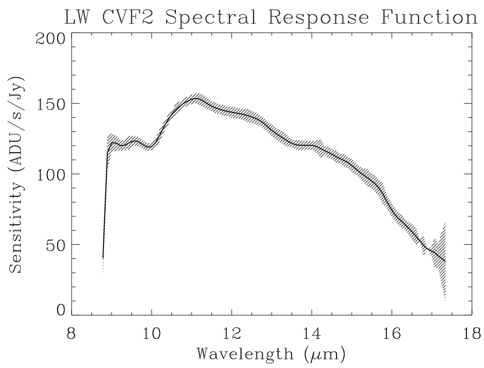

Figure 5. The LW CVF2 SRF within its $\pm 1\sigma$ confidence range (shaded region), where σ is the RMS obtained from the several measurements used to obtain the SRF. Note that the use of the CVF2 positions at $\lambda < 9.003\mu m$ and $\lambda > 16.52\mu m$ is not recommended.

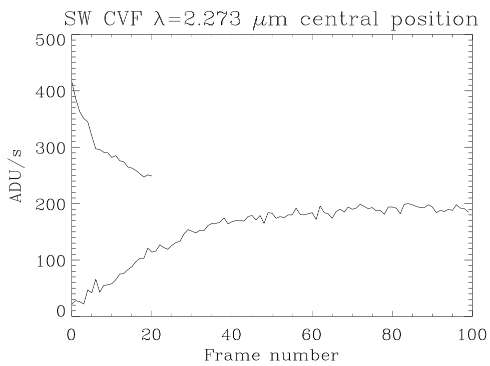

Figure 6. The signal time histories of the brightest pixel of the HIC96441 star image, at the first SW CVF position, observed during a forward (short to long wavelengths) scan, and a following backward scan. The first time the pixel sees the star, during the forward scan, the signal is stabilizing upwards and is possibly stabilized after ~ 100 frames; the second time, there is a downward stabilizing trend but the observation is too short to allow complete stabilization.

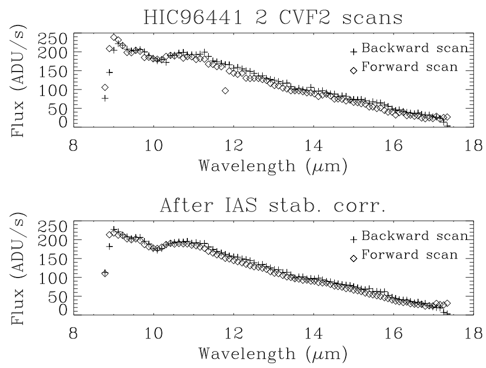

Figure 7. The spectrum of the star HIC96441 observed twice with once in a forward scan from short to long wavelengths, and immediately after in a backward scan. The top panel show the spectrum obtained without any transient correction. The bottom panel show the spectrum derived using Abergel et al.'s transient correction.

100 frames per step would have been too much time consuming. The consequence of this (forced) choice is the incomplete downward stabilizing trend of the same pixel signal when the same star is observed again at the same CVF position, at the end of the backward scan, started after the forward scan (from short to long wavelengths) was completed. The downward stabilizing trend is due to the fact that a higher flux was falling onto that pixel in the previous position, because the CVF is much less sensitive at the first position than at the second one while the star flux is similar. It is clear that stabilization is not achieved yet, and, more importantly, the two observations do not converge to the same signal. The total flux derived for the star at this CVF position was 238 ADU/s on the forward scan, but much higher (404 ADU/s) on the backward scan.

Currently available models for transient-correction can however help to improve the situation. An example of this is shown in Fig. 7, where we plot the fluxes of the star HIC96441 obtained in two consecutive CVF2 scans (forward and backward), before and after the transient correction developed by Abergel, Désert and Aussel was applied. The relatively large flux differences between the forth and the back scans are diminished, and overall the star spectrum looks less noisy, after the transient correction is applied. Note however that observations of our primary calibrating star, HIC94376, suffer much less from transient effects, because its flux is much higher than the flux of HIC96441 (more than a factor 10).

We have not yet applied a transient correction model to all our calibration observations, because the model is still being refined. However, the examples given above show that our current understanding of the transient behaviour of CAM pixels is good, and that we expect to further improve upon this topic in the near future.

2.2. Absolute flux calibration: γ Draconis

The very bright star HIC87833, or γ Draconis, has been observed with CVF2 in rev.482, for the purpose of cross-calibration with other ISO instruments (PHT and SWS) and for a comparison with a composite spectrum assembled from ground-based and KAO observations (Cohen et

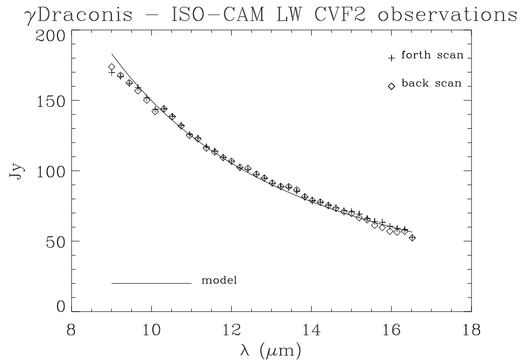

Figure 8. The spectrum of the star γ Draconis observed twice with the LW CVF2, once in a forward scan from short to long wavelengths, and immediately after in a backward scan. The line shows a composite spectrum derived from non-ISO observations by Cohen et al. (1995).

al. 1995, AJ, 110, 275), data from the IRAS Point Source Catalogue and an IRAS Low Resolution Spectrum. Here we quote results of the comparison of our CAM observations with the composite spectrum from Cohen et al.

In Fig. 8 we show the spectrum of this star (in Jy) as obtained through two consecutive forward and backward scans, as compared with Cohen's composite spectrum. It can be seen that the CAM spectrum agrees with the composite spectrum over all the range of observed wavelengths (9 to 16.5 μm). The maximum deviations seen are at the long wavelength edge position of the CVF2 (7 %), where the spectral response function may still be far from perfect, because the calibrator fluxes are low, and at around 11 μm (3 %); there is no average systematic deviation and the rms deviation is only 2 %. This is fully consistent with the accuracy of the CVF2 SRF (see § ??).

3. Ghosts

Ghost-images are important in CVF. This was expected since, at variance with CAM filters, the CVF could not be tilted with respect to the optical axis. The presence of ghost-images affects the photometry and the imaging.

In Fig. 9 I have plotted three independent observations of the same star, δ Draconis, done with CVF at $\lambda = 7.414 \mu m$ In order to show the ghosts, I have plotted logarithmic intensity scales. In one of the observations, the star image is at the centre of the array, in the other two, it is at the left and right edges. Two types of ghost-images can be seen. One has a ring-shape and is comoving with the source image. The other has a circular shape and moves symmetrically with respect to the CAM array centre, as the source moves. I will call the two kinds of ghost the *comoving* ghost and the *symmetric* ghost, respectively.

The results of aperture photometry on the source and the ghost images are shown in Fig.10 and Fig.11 for the CVF1 and, respectively, the CVF2. We can notice that the *comoving* ghost spectrum looks similar to the source spectrum, except maybe at the short-wavelength edge of the CVF1, and at the long-wavelength edge of the CVF2. The *symmetric* ghost spectrum seems significantly differ-

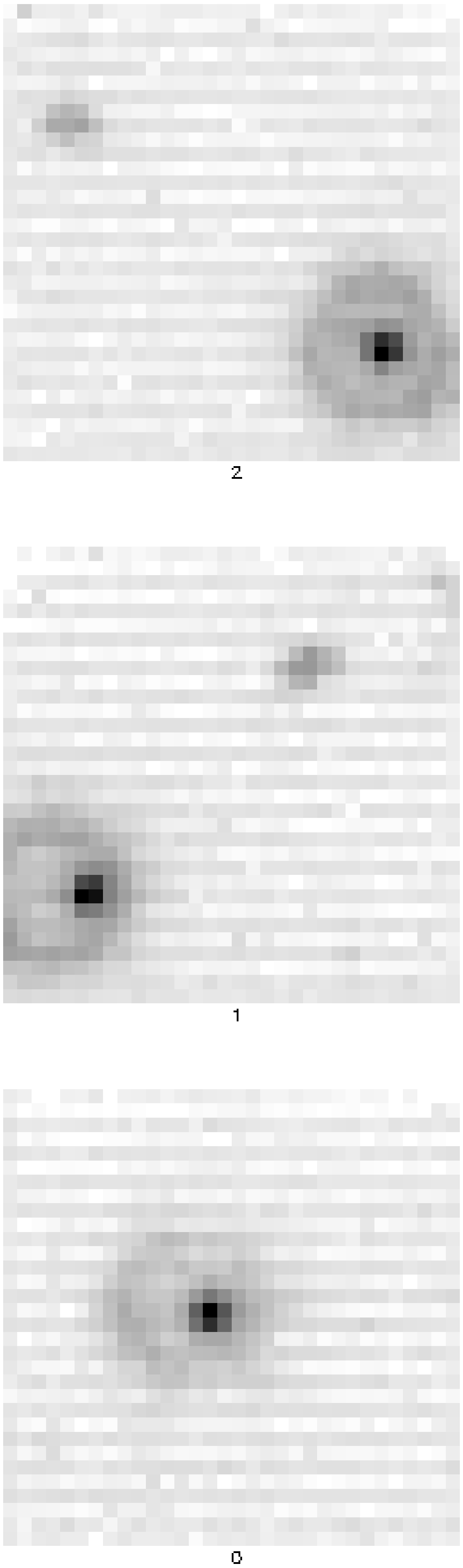

Figure 9. Ghost images in the three CVF observations δ Draconis.

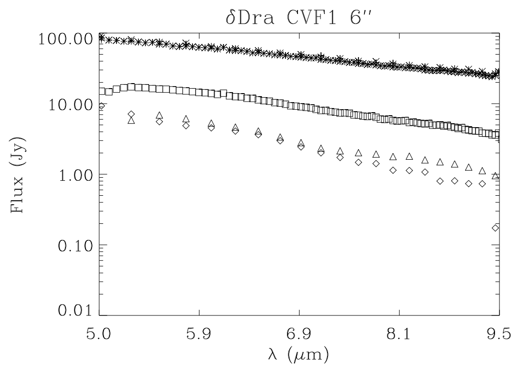

Figure 10. Aperture photometry on the star δ Draconis and its ghost images with the CVF1. Asterisks, pluses, and X's indicate three independent measurements of the star fluxes; squares indicate measurements of the comoving *ghost fluxes; triangles and diamonds indicate measurements of the* symmetric *ghost fluxes, at the left and the right off-centre positions. Scales are logarithmic.*

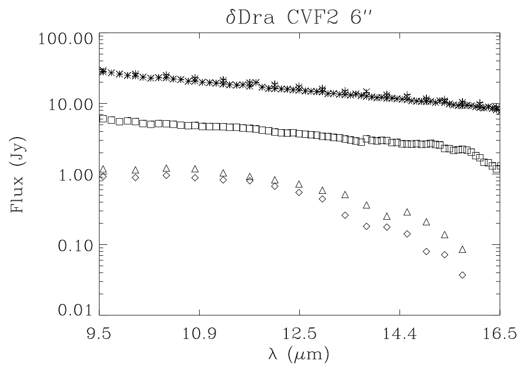

Figure 11. Aperture photometry on the star δ Draconis and its ghost images with the CVF2. Asterisks, pluses, and X's indicate three independent measurements of the star fluxes; squares indicate measurements of the comoving *ghost fluxes; triangles and diamonds indicate measurements of the* symmetric *ghost fluxes, at the left and the right off-centre positions. Scales are logarithmic.*

ent from the source spectrum at long wavelengths with the CVF2. It is noticeable that the spectra measured for the *symmetric* ghost, on the left and on the right offset positions, are almost identical.

The ratio between the ghost and the star flux is ~ 20 %, on average, for the *comoving* ghost, and only ~ 4 % for the *symmetric* ghost.

4. Spectral purity

From observations of Planetary Nebulae taken during the PV-phase, the central wavelengths of two lines, NeII and SIV were derived (by simple gaussian fitting over the continuum). They were found to fall at the expected CVF position, within a few hundreths of a CVF step. Transient effects may slightly change the observed position of the line, by less than a tenth of a CVF step.

The wavelength purity is reduced when the source is not centered in the middle of the array. An analysis of the

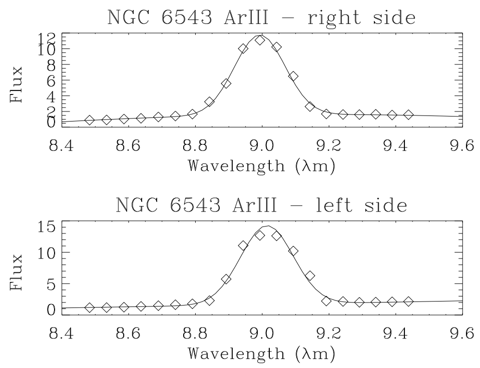

Figure 12. The spectrum of NGC 6543 around the ArIII line, as observed with the source put on the right side (top panel) and the left side (bottom panel) of the CAM detector.

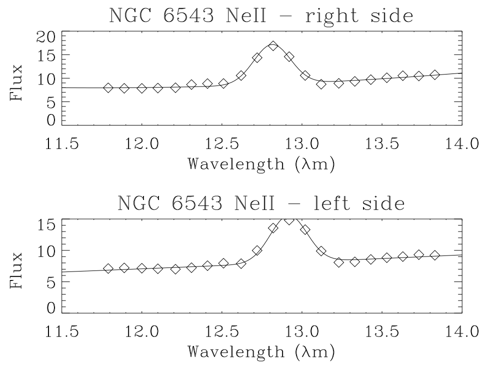

Figure 13. The spectrum of NGC 6543 around the NII line, as observed with the source put on the right side (top panel) and the left side (bottom panel) of the CAM detector.

NeIII-line central position in a CAM CVF image of the M17 planetary nebula, has shown that the central observed wavelength position of the NeIII line is 0.09 μm higher at the left edge of the CAM array than at the centre. At the position of the CVF2 corresponding to the wavelength of the NeIII line (15.555 μm), such a shift corresponds to roughly a CVF step. At the right edge, however, there is no significant wavelength shift.

On the other hand, there is no wavelength-dependence on the top-down direction of the array, as expected from the orientation of the CVF with respect to the array.

These results are confirmed by independent observations of the NGC 6543 planetary nebula, whose image was positioned on the left and right edges of the CAM detector (on purpose, to check the CVF wavelenght calibration). In Fig.12 and Fig.13 I show the spectrum of NGC 6543 as obtained with the CVF on the two CAM edge positions, around the wavelength of the ArIII line, and the NeII line, respectively. It is clear that when the source image is located on the right edge of the detector there is no significant wavelength shift, while when the source is located on the left edge of the detector, the shift is siginificant, and equal to 0.023 μm at the wavelength of the ArIII line, 8.991 μm, and to 0.109 μm at the wavelength of the NeII line, 12.814 μm. These results are consistent with those found for M17. In addition, there is an indication that the wavelength-shift is wavelength-dependent, being larger at higher wavelengths.

Further investigation is needed on this topic to achieve a full calibration of the CVF spectral purity. Currently available observations of extended sources will be used to map the wavelength-shift of the CVF observations over the CAM array.

5. Conclusions

I have shown that the SRF of the CVF is currently well constrained, to within ± 4 % average rms. New versions of the calibration files will include a theoretical PSF-correction of the SRF. The *measured* PSF in several CVF positions is affected by the presence of ghost images, so it is safer to use the theoretical PSF, until a full understanding of the ghost properties is achieved.

The correction for the ghost images can be important. I have shown that neglecting the contribution of the ghost can significantly affect the photometric results (by ~ 25 %). Currently many people are involved in the development of an optical model of the telescope and the CAM optics to address the problem of ghost. With the already available observations, we will be able to calibrate the extent, intensity and positions of the ghost images in the CVF.

Finally, for what concerns the CVF spectral calibration, I have pointed out that it is very accurate when the source image is located at the centre of the array, but there is a systematic wavelength shift of up to $+1$ CVF step positions, when the source image is located on the left of the CAM array. No shift is observed to the right of the detector. New calibrations are needed of this effect in order to actually map this wavelength dependence for all CAM pixel positions.

ACKNOWLEDGMENTS

This paper could not have been written without the significant contribution of many people. I wish to give a special thank to Alain Abergel, François Boulanger, Diego Cesarsky, and Bill Reach from the *Institut d'Astrophysique Spatiale,* in Orsay, and to all my colleagues of the *CAM Instrument Dedicated Team* in Villafranca.